Composite Structures 220 (2019) 940–952

Contents lists available at ScienceDirect

Composite Structures

journal homepage: www.elsevier.com/locate/compstruct

Strengthening of reinforced concrete structure using sprayable fiber-reinforced cementitious composites with high ductility

Bo-Tao Huang[a], Qing-Hua Li[a,*], Shi-Lang Xu[a], Bin Zhou[b]

[a] Institute of Advanced Engineering Structures and Materials, Zhejiang University, Hangzhou 310058, China
[b] The Personnel Education Department, Ministry of Transport of the People's Republic of China, Beijing 100736, China

ARTICLE INFO

Keywords:
Spray
Fiber-reinforced
ECC
SHCC
Strengthen
Application

ABSTRACT

Fiber-reinforced cementitious composites with high ductility exhibit significant pseudo-strain-hardening response and multi-cracking behavior. In this paper, a systematical investigation of a sprayable fiber-reinforced cementitious material with high ductility is presented from material design to practical application. This sprayable material is formed using the wet-mix spray process, and its compressive, tensile, and flexural strengths are higher than those of the cast ones with the same proportion. A series of reinforced concrete beams, including unloaded and pre-loaded ones, is strengthened with this material, and the four-point bending test is performed to evaluate the flexural performance of the composite elements. A theoretical analysis is conducted to predict the load capacity of the specimens. The application cases of this sprayable material in China are presented to show its potential application in the construction of durable concrete structures and restoration of aged structures.

1. Introduction

Reinforced concrete is most widely used in the structures in modern infrastructures worldwide. For a concrete material, one of its major limitations is its quasi-brittle behavior, which may contribute significantly to the cracking of concrete structures and reduction in their durability. Although the brittle performance of concrete is significantly decreased by the inclusion of fibers, most fiber-reinforced concrete has a low tensile strain capacity (i.e., approximately 0.01%). The localization of the damage in this material occurs after the first cracking, which leads to a tension-softening behavior under tension. In recent decades, fiber-reinforced cementitious composites with high ductility have been developed based on the micromechanics principles proposed by Li and Leung [1]. Such a material exhibits significant pseudo-strain-hardening response and multi-cracking behavior and is also referred to as engineered cementitious composites (ECCs) [2–5], strain-hardening cementitious composites (SHCCs) [6–8], or ultra-high toughness cementitious composites (UHTCCs) [9–11]. A UHTCC possesses a much higher ductility under both monotonic and fatigue loadings compared with conventional concrete [12–17], and it has potential applications for improving the mechanical performance and durability of concrete structures [18–22].

For the structural application of a UHTCC, substituting the normal concrete by the UHTCC in the whole structure would lead to a significantly higher cost because the polymeric fibers used in a UHTCC are much more expensive than cement, sand, or water. A strategically effective solution to this problem is the partial use of this material at crucial locations in the concrete structures. Thus, a UHTCC functionally-graded structure was proposed [23]. This composite structure utilizes the strain-hardening property of UHTCCs to limit the crack width of the reinforced concrete members. It also made it possible to prevent the migration of aggressive substances into the concrete or reinforcement [23,24] and improve the loading capacity of the concrete member [20,21]. Hence, the application of a UHTCC in the construction and restoration of reinforced concrete structures is promising. However, the construction of a UHTCC functionally-graded structure is more complex than that of a normal reinforced concrete structure. For the sake of efficiency, sprayable UHTCCs were proposed by Kim et al. [25] and Kanda et al. [26], which have the advantages of reduced formwork and faster construction.

In the past decade, numerous efforts have been made for the development of sprayable UHTCCs and their applications [25–31]. Kim et al. [25,27,28] proposed a sprayable UHTCC based on the parallel control of micromechanics- and rheology-based designs, and they investigated the mechanical properties and repair performance of this material. Kanda et al. [26] developed a direct sprayable UHTCC and found that this material had the potential for prolonging the service life of reinforced concrete members in a heavy chloride environment. A

* Corresponding author.
E-mail addresses: botaohuang@zju.edu.cn (B.-T. Huang), liqinghua@zju.edu.cn (Q.-H. Li), slxu@zju.edu.cn (S.-L. Xu).

https://doi.org/10.1016/j.compstruct.2019.04.061
Received 17 August 2018; Received in revised form 5 April 2019; Accepted 12 April 2019
Available online 13 April 2019

sprayable UHTCC was used to protect the deteriorated concrete surface of an aged dam structure (Mitaka Dam, Japan), and it was applied in the restoration of a railway viaduct possessing flexural fatigue cracks [29]. Li et al. [30] reported the application of a sprayable UHTCC in the repair of tunnels, including the replacement of chloride-infested concrete and in coating as a protective layer for a damaged lining. Recently, Zhang and Li [31] developed a novel spray-applied fire-resistive UHTCC, which combined the properties of a desirable thermal insulation, sprayability, and lightweight. The existing literature has extended the knowledge of sprayable UHTCCs and their application. However, the experimental and theoretical investigations of sprayable-UHTCC-strengthened reinforced concrete elements, including damaged and undamaged ones, are still limited. The mechanical response of the sprayable UHTCC layer in a reinforced concrete element is important for the further application of this material. Additionally, the investigation of the effect of different spray methods (e.g., single-layer spray and layer-by-layer spray) on the performance of this material is also essential for its large-scale application.

In this paper, a systematical investigation of a sprayable UHTCC-strengthened reinforced concrete structure is presented, starting from material design to practical application. The sprayable UHTCC was first formed using the wet-mix spray process, and the compressive, tensile, and flexural behaviors were investigated. A series of reinforced concrete beams, including unloaded and pre-loaded ones, was strengthened with a sprayable UHTCC layer, and the four-point bending test was performed to evaluate the effect of the UHTCC on the flexural performance. A theoretical analysis was conducted to calculate the steel-yield and ultimate load capacities of the specimens. Construction and restoration cases in China using the sprayable UHTCC were also briefly introduced to show the potential application of this material. Finally, relevant conclusions were drawn.

2. Sprayable UHTCC

The sprayable UHTCC in this study is a low-velocity-sprayed mortar, which is not shotcrete. Compared to conventional sprayable fiber-reinforced concrete, UHTCC has a higher fiber volume fraction (2%) and has no coarse aggregate. The differences may result in the difference of the spray techniques. Although the standards of shotcrete (e.g., ACI Guide to Shotcrete [32], EFNARC European Specification for Sprayed Concrete [33]) can provide important guidance, they might be more suitable for fiber-reinforced concrete than UHTCC. It is known that UHTCCs are a unique group of high-performance fiber reinforced cementitious composites (HPFRCCs) distinguished by extraordinary tensile ductility with moderate fiber content. In this study, the spraying process is referred to the JSEC's "Recommendations for design and construction of high performance fiber reinforced cement composites with multiple fine cracks (HPFRCC)" [34]. In JSEC's "Recommendations", there is one chapter focused on spray technology. The experimental research in this study was mainly referred to the JSEC's "Recommendations" and the other previous work on sprayable UHTCC (e.g., [25,27]).

2.1. Materials

In this study, the sprayable UHTCC was produced using cementitious binders, water, fine silica sand, polycarboxylate superplasticizer (SP), hydroxypropyl methylcellulose (HPMC), and polyvinyl alcohol (PVA) fibers. The cementitious binders included ordinary Portland cement (P·O 52.5, corresponding to the Chinese standard GB175-2007) and fly ash (Class F). The composition of the matrix of the sprayable UHTCC was cementitious binders: water: fine sand = 1: 0.3: 0.2. The maximum aggregate size of the silica sand was 300 μm. The ratio of SP and HPMC to the cementitious binders was 0.075% and 0.1% (by weight), respectively. The properties of the PVA fiber are listed in Table 1, and the fiber volume fraction was 2.0%. The spray process of UHTCC is illustrated in Fig. 1. The mixing process of fresh UHTCC is as follows: 1) the cementitious binders and fine silica sand are added to the mixer, and the mixing is for 1 min; 2) the SP and HPMC are added and mixed for 2 min, 3) the PVA fibers are added and mixed for 2–3 min. Then, the freshly prepared UHTCC was pumped through a rubber hose to a spray gun. It needs to be pointed out that the element accelerating the setting time was not used in this sprayable UHTCC. Because it is found that the proposed sprayable UHTCC already shows enough bonding with the substrate and the rebound rate is low during the spray process of the experimental tests and application cases, which are shown in the following sections. Actually, according to the former research (e.g., Ref. [25]), the element accelerating the setting time (e.g., calcium aluminate cement) can be applied in the sprayable UHTCC and the fresh and hardened behaviors of sprayed UHTCC are stable.

Table 1
Properties of the PVA fiber.

Property	Value
Tensile strength (MPa)	1600
Diameter (μm)	40
Fiber length (mm)	8
Young's modulus (GPa)	40
Elongation (%)	6

2.2. Sprayable performance and spray process

During the spray process, fresh UHTCC was sprayed with an air flow of approximately 0.1 m^3/min to 0.3 m^3/min and an air pressure of 600 kPa to 200 kPa, and the distance between the spray gun and concrete substrate was approximately 0.2–0.5 m. It should be pointed out that the air pressure is the compressor internal pressure, which was measured by the pressure sensor of the compressor. The statuses of the sprayable UHTCC with different air pressures are presented in Fig. 2. A narrow stream of the sprayable UHTCC is observed with the air flow of approximately 0.3 m^3/min and the air pressure of 200 kPa (shown in Fig. 2(a)), whereas foggy-like sprayable UHTCC can be seen with the air flow of approximately 0.1 m^3/min and the air pressure of 600 kPa. During the construction or maintenance of concrete structures, the narrow-stream-like sprayable UHTCC may be applied in some narrow areas, while the foggy-like sprayable UHTCC may be utilized in some large areas. Additionally, it is found that the adhesion of the sprayable UHTCC and concrete substrate is adequate. According to the reference [35], the spray process of UHTCC is a low-velocity spray compared to the high-velocity spray of the shotcrete process.

A brief spray process of the UHTCC is illustrated in Fig. 3. First, the surface of the concrete substrate is cleaned using a water jet (Fig. 3(a)). Then, the UHTCC is sprayed with an air flow of approximately 0.12 m^3/min and an air pressure of 500 kPa (Fig. 3(b) & (c)). Finally, the surface of the sprayable UHTCC is smoothed, and the spray process is completed (Fig. 3(d)). It is found that the rebound rate of the sprayable UHTCC is lower than 5%. The rebound rate was measured with an overhead spray process (thickness of UHTCC layer approximately 25 mm). The mass of the receiving surface was measured by an electronic balance before and after the spray process to obtain the mass of UHTCC attached to the substrate (m_1). Then, the rebound UHTCC was collected on a tarp and measured on the electronic balance to obtain the mass of the rebound UHTCC (m_2). The value of $m_2/(m_1 + m_2)$ was calculated as the rebound rate. In addition, for overhead spraying, the maximum thickness of sprayed UHTCC is approximately 30 mm and the recommendation value is 20 mm. For vertical spraying, the maximum thickness of sprayed UHTCC is approximately 50 mm and the recommendation value is 40 mm.

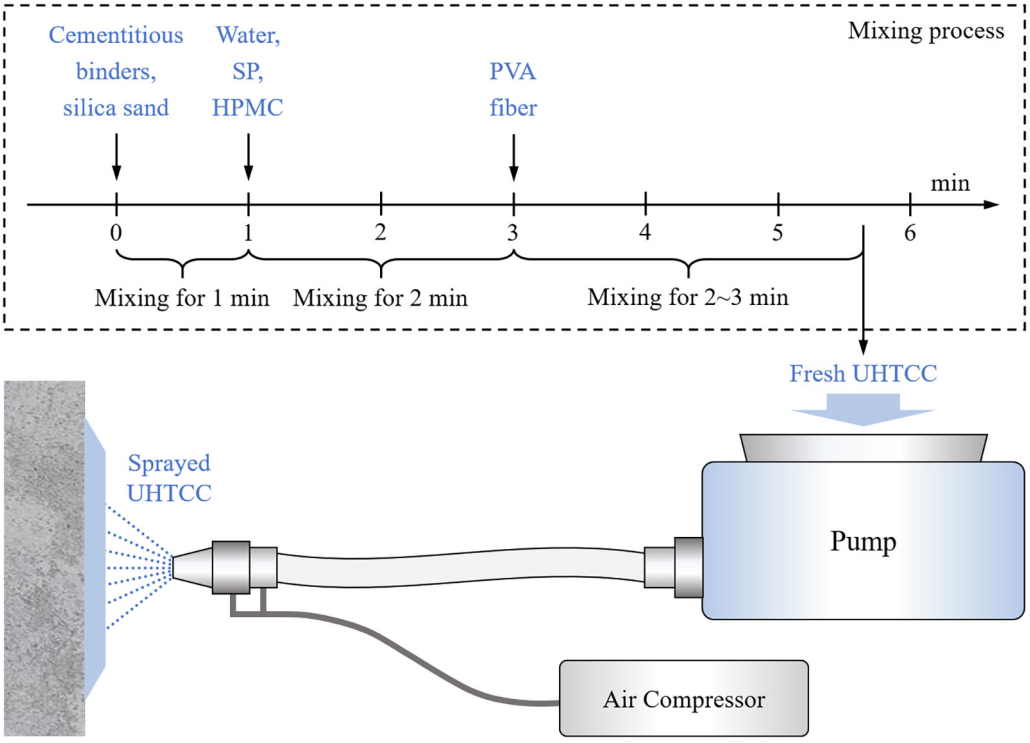

Fig. 1. Mixing and spray processes of the sprayable UHTCC.

2.3. Mechanical performance of sprayable UHTCC

2.3.1. Specimen preparation

The specimens shown in Fig. 4 are prepared to evaluate the mechanical performance of the sprayable UHTCC, including the compressive, tensile, and flexural performance. These panels were demoded two days after the spray process, and they were laid in ambient environment (temperature: 15–20 °C, relative humidity: approximately 75%) up to the test date. Before the mechanical tests, the specimens were cut from the sprayable UHTCC panels. The detailed dimensions of the cut specimens are listed in Table 2. It should be noted that UHTCC is a micromechanically designed fiber-reinforced cementitious material and the fiber/matrix interactions and the flaw size distribution of the matrix have a significant influence on the strain-hardening and multi-cracking responses of this material. For the cast-in-place and sprayed UHTCC, these two factors may be different, which may result in the variation of the mechanical response. An understanding of the influence of the spray process on the mechanical behavior of UHTCC is useful to further design and optimization of the sprayable UHTCC. Hence, specimens using cast UHTCC were also prepared for comparison. For the sprayed and cast UHTCC, the same mix proportion was used and the only difference between them was the producing processes. According to the ASTM standard [36], the apparent density of the sprayable UHTCC was 1760 kg/m^3, which was higher than that of the cast UHTCC (1670 kg/m^3). A similar phenomenon was also reported in the former works on sprayable mortars and UHTCCs [27,37]. This trend is most probably related to the pneumatic compaction during the spray process [27].

2.3.2. Compressive, tensile, and flexural performance

For the UHTCC-strengthened concrete component, the tensile and flexural performance of UHTCC is more important than its compressive performance. For the compressive performance, only the load capacity of UHTCC was investigated in this study and hence load control was used during the test. For the tensile and flexural performance, both of the load and deformation capacities were investigated and hence displacement control was used. The displacement control is generally used in the tensile and flexural test of UHTCC to obtain its deformation

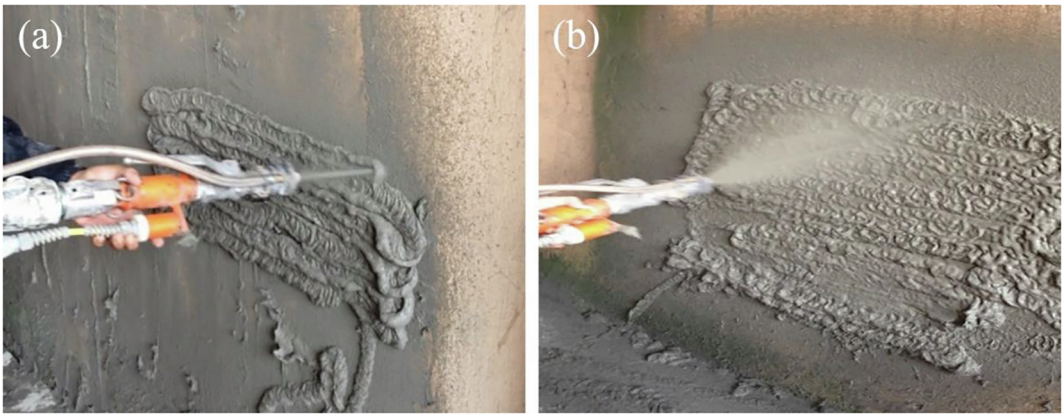

Fig. 2. Sprayable UHTCC at different air pressures: (a) approximately 0.3 m^3/min and 200 kPa; (b) approximately 0.1 m^3/min and 600 kPa.

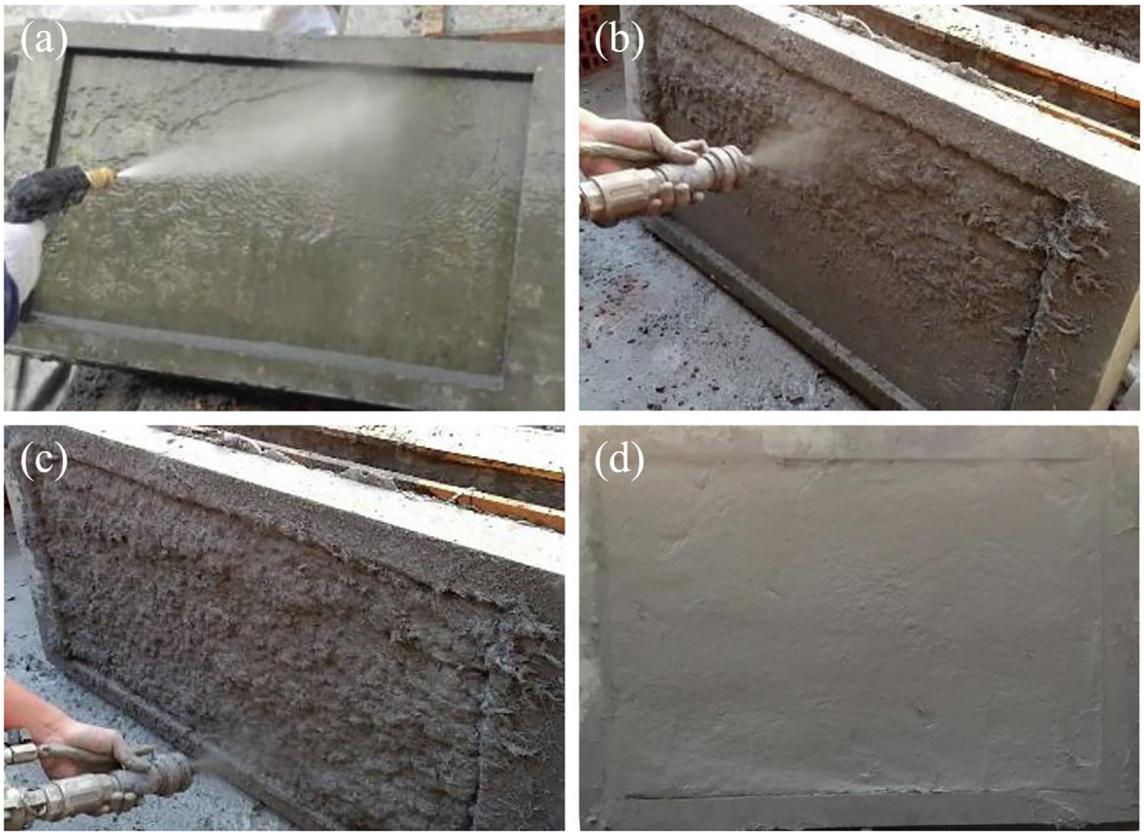

Fig. 3. Spray process of the UHTCC: (a) the surface of the existing concrete is cleaned using a water jet; (b) UHTCC is sprayed; (c) spraying is completed; (d) the surface is smoothened.

capacity, which is referred to the former research and recommendation of the cast and sprayed UHTCC [27,34,38,39].

In the compressive test, a 1000-kN-INSTRON testing system was used. Load control was adopted with a constant rate of 5 kN/s. The compressive strengths of the sprayed and cast UHTCC were measured at 7 d, 14 d, and 28 d, and three specimens were tested for each group. The average strengths are presented in Fig. 5. It can be found that the compressive strength of the sprayable UHTCC is higher than that of the cast one. This phenomenon may be related to the fact that the density of the sprayable UHTCC is higher than that of cast UHTCC, which leads to a lower porosity of the sprayable UHTCC.

The tensile test was performed in a 250-kN-INSTRON testing system. Displacement control was used with a constant rate of 0.1 mm/min. In this experiment, two linear variable differential transformers (LVDTs) were fixed to the specimen to obtain the tensile deformation at a 150-mm-gauge length. The tensile stress-strain curves of the sprayable UHTCC (i.e., S-UHTCC) and cast UHTCC (i.e., C-UHTCC) were obtained at 14 d and 28 d (shown in Fig. 6). It can be found that the tensile strength of the sprayable UHTCC is higher than that of the cast UHTCC at both 14 d and 28 d. In addition, the tensile strain capacity of the sprayable UHTCC is also higher than that of the cast UHTCC. It is known that the flaw size distribution affects the multiple cracking behavior of a UHTCC [40]. Owing to the pneumatic compaction during the spray process, the flaw size distribution of the sprayable UHTCC may be different from that of the cast UHTCC, which causes the variation in the tensile strain capacity. However, no direct evidence was obtained in this study regarding this, and further investigation of this phenomenon is required in a following work.

The three-point bending test was also performed in a 250-kN-INSTRON testing system. Displacement control was used with a constant rate of 0.2 mm/min. The support span of the tested beam specimen was 120 mm, and a pair of LVDTs were used to measure the mid-span deflection. The flexural stress *vs.* deflection curves of the sprayed and cast UHTCCs were obtained at 14 d and 28 d (shown in Fig. 7). It can be found that the flexural strength and deformation capacity of the sprayable UHTCC are higher than those of the cast UHTCC at both 14 d and 28 d. This can be explained by the fact that the sprayable UHTCC shows better compressive and tensile performances than the cast UHTCC.

3. Reinforced concrete beams strengthened by sprayable UHTCC

3.1. Experimental program

In this section, a series of reinforced concrete (RC) beam specimens were prepared with a sprayable UHTCC layer, and the four-point bending test was performed to evaluate the effect of the UHTCC on the flexural performance of the RC beam. Fig. 8 presents the details of the beam specimens and bending test. The detailed specimen ID and dimensions are listed in Table 3. The beam specimens are shown in Fig. 8(a) and (b) are composed of RC and a sprayable UHTCC layer (i.e., UH0, UH10, UH20, and UH20(2) in Table 3). The thicknesses of the UHTCC layer are 0 mm, 10 mm, and 20 mm, and the height of the beam specimens (including the UHTCC layer) is 200 mm. It should be pointed out that the UHTCC layers in UH0, UH10, and UH20 in Fig. 8(a) are single-layer sprayed, whereas that in UH20(2) in Fig. 8(b) is layer-by-layer sprayed (each time 10 mm UHTCC is sprayed at a time interval of one day). UH20(2) is prepared to investigate the effect of different spray methods on the load capacity of the RC–UHTCC beams. Fig. 8(c) displays the pre-loaded RC beams (with a height of 200 mm) strengthened by different thicknesses of the sprayable UHTCC layer (i.e., 5 mm and 10 mm). Thus, the heights of these strengthened specimens (i.e., UH0 + 5 and UH0 + 10) are 205 mm and 210 mm, respectively. It needs to be pointed out that after the fabrication of the

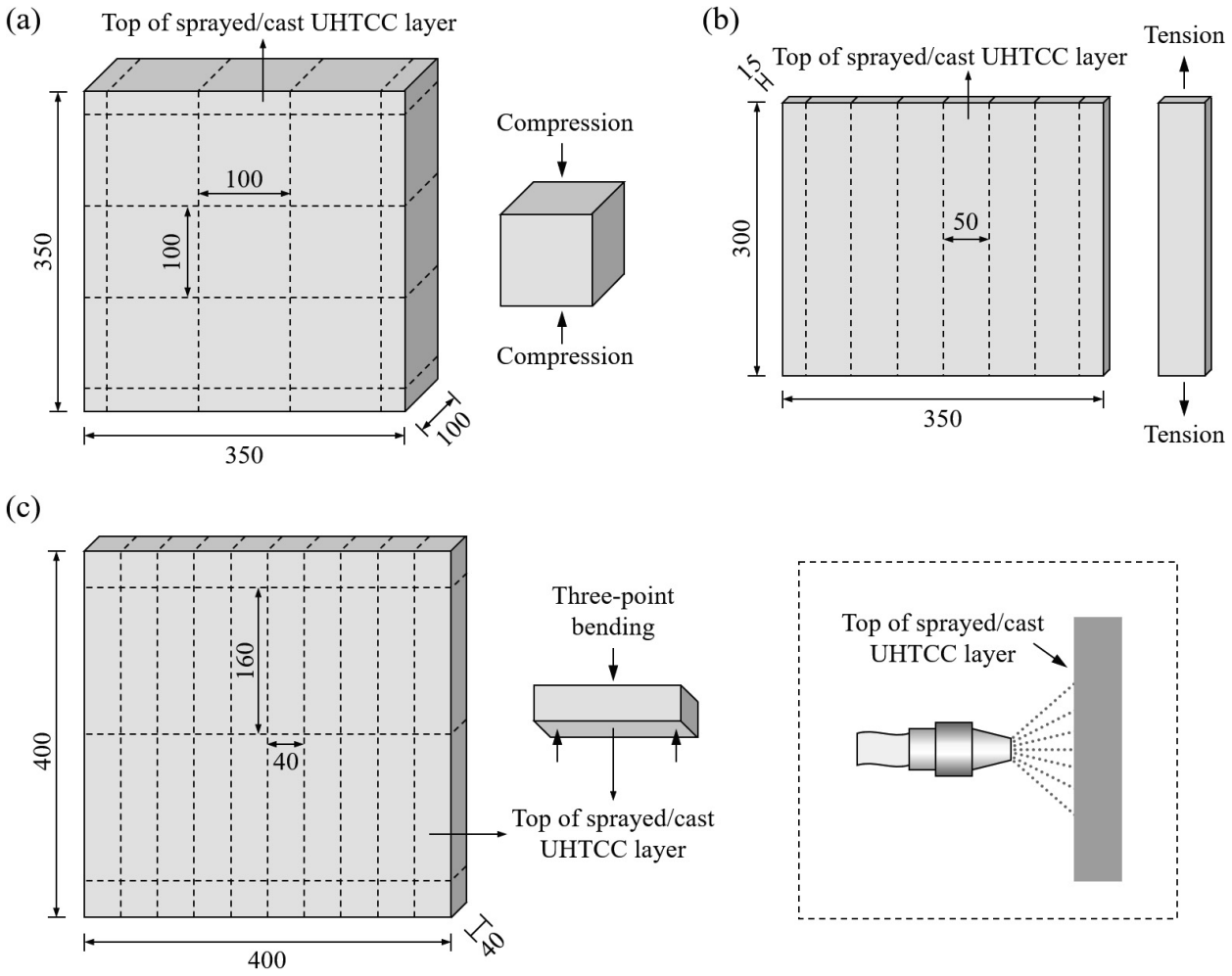

Fig. 4. Preparation of the specimens to determinate the (a) compressive, (b) tensile, and (c) flexural performance of the sprayable UHTCC.

Table 2
Dimensions of the specimens.

Mechanical tests	Specimen dimensions (mm)
Compression	100 × 100 × 100
Tension	300 × 50 × 15
Flexure	160 × 40 × 40

reinforced concrete layers of the beam specimens, formworks were still utilized to guarantee the different thicknesses of the sprayed UHTCC layers. For each specimen, the plain concrete and reinforcement were the same. The compressive strength of plain concrete was 26.7 MPa, the yield strength of the longitudinal bars in tension zone (12 mm diameter) was 391 MPa, and the yield strength of the steel bars in compression zone (8 mm diameter) was 280 MPa. The sprayable UHTCC prepared as discussed in Section 2 was used to strengthen the RC beams shown in Fig. 8.

The timeline of the specimen preparation and bending test is presented in Fig. 9. First, the RC layer of each specimen is prepared and cured for 28 d. Second, the UHTCC layers are sprayed to fabricate specimens UH10, UH20, and UH20(2). For the specimens UH10 and UH20, the UHTCC layers are sprayed in one time. For the specimen UH20(2), UHTCC is layer-by-layer sprayed (each time 10 mm UHTCC is sprayed at a time interval of one day). Third, the bending tests of UH0, UH10, UH20, and UH20(2) are performed after curing, and the two RC beams prepared for UH0 + 5 and UH0 + 10 are pre-loaded using the average yield load of UH0. Finally, after the preloading, the UHTCC layers are sprayed on the unloaded RC beams to fabricate the specimens UH0 + 5 and UH0 + 10, and they are tested after curing for another 28 d. In the bending test, a 1000-kN-INSTRON testing system is used. The four-point bending test is performed under a displacement control of 0.2 mm/min. A pair of LVDTs are used to obtain the mid-span deflection of the beam specimens.

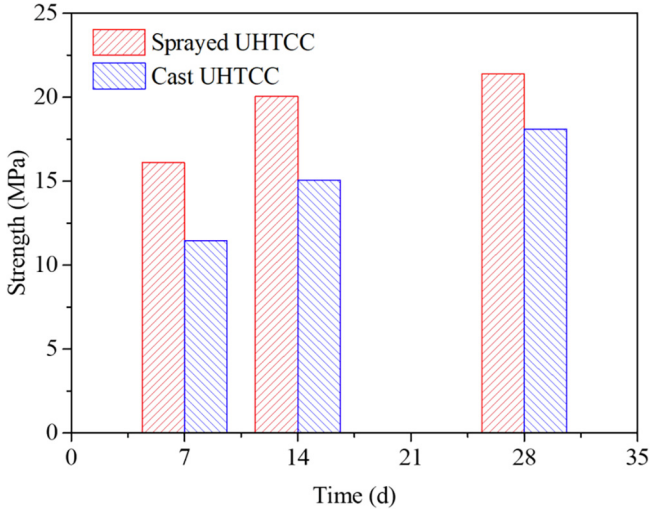

Fig. 5. Compressive strength of the sprayed and cast UHTCCs.

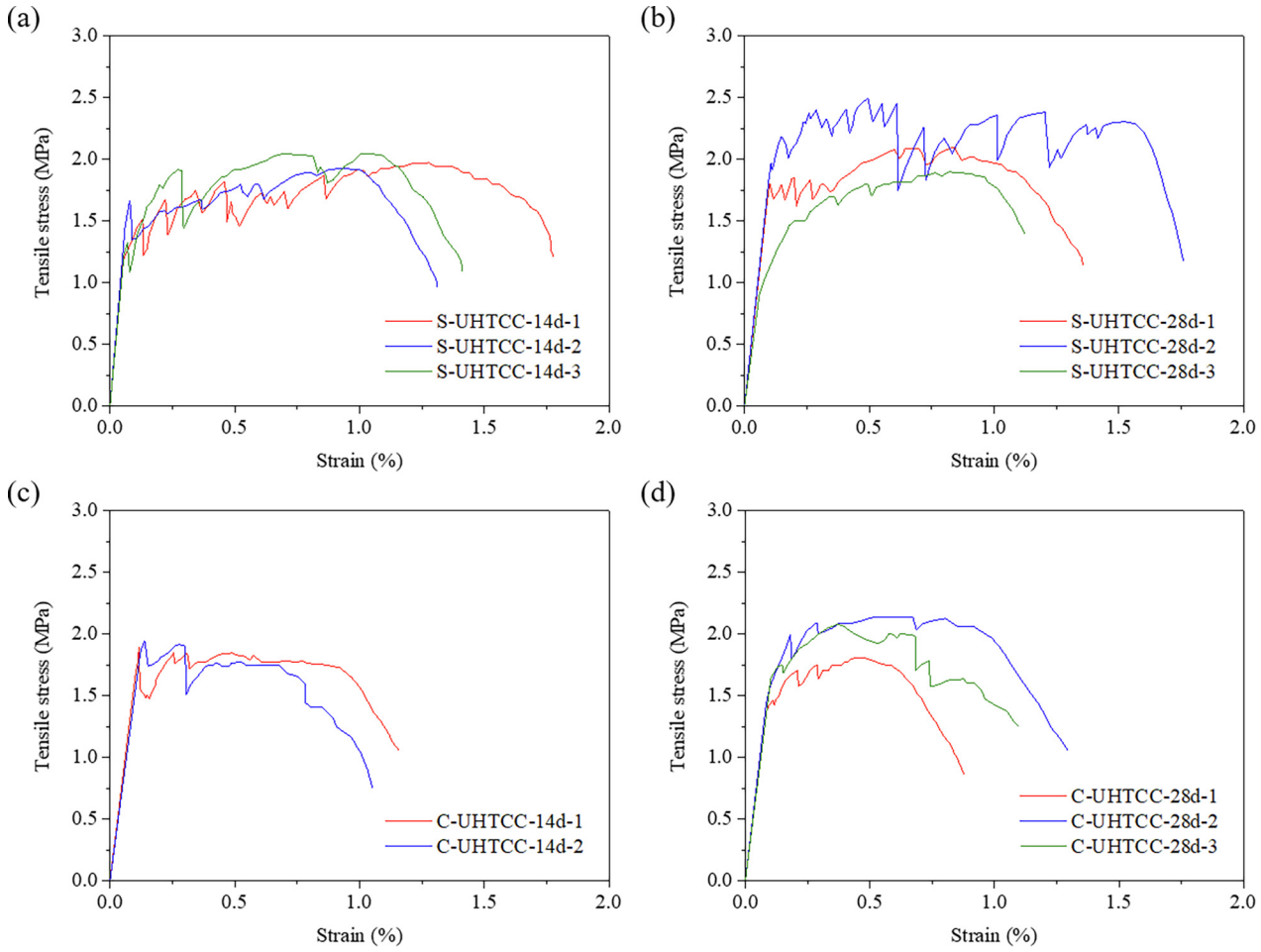

Fig. 6. Tensile stress *vs.* strain curves: (a) sprayable UHTCC at 14 d; (b) sprayable UHTCC at 28 d; (c) cast UHTCC at 14 d; (d) cast UHTCC at 28 d.

3.2. Test results of UH0, UH10, and UH20

The load *vs.* mid-span deflection curves of UH0, UH10, UH20, and UH20(2) are exhibited in Fig. 10 along with the average curve of each group. It can be seen that the stiffness, steel yield load, and ultimate load of the beam specimens increase as the thickness of the UHTCC layer increases. This phenomenon can be explained by the tensile strain-hardening response of the sprayable UHTCC [21,41], which is seen previously in Fig. 6. Also, the strain-hardening response of UHTCC can increase the slope of the post-yielding branch of the beam specimens. The tensile strength of the UHTCC in a cracked state can still contribute to the load capacity of the beam components under monotonic loading [10,21], whereas that of conventional concrete is typically neglected. It can also be observed in Fig. 10(d) that the load *vs.* mid-span deflection curves of UH20 and UH20(2) are very close. Additionally, interface delamination is not observed between the two UHTCC layers in UH20(2). This indicates that the layer-by-layer spray process for the UHTCC may have little effect on the load capacity of the beam specimen as opposed to the single-layer spray process.

The local cracks in UH20-1 at the load of 60 kN are shown in Fig. 11. It can be observed that the cracks in the RC layer become multiple cracks in the UHTCC layer (see Fig. 11(a)). A similar phenomenon is also reported in former works [20,22]. The crack width in the RC layer is approximately 0.24 mm (see Fig. 11(b)), whereas that in the UHTCC layer is only approximately 0.02 mm. This indicates that the sprayable UHTCC layer can effectively control the crack in the concrete layer, and thus, it can be employed as a protective layer for an RC element.

For each group of the specimens (i.e., UH0, UH10, UH20), the development of the maximum crack width in the concrete layer is presented in Fig. 12. It can be seen that the maximum crack width in the concrete decreases as the thickness of the UHTCC layer increases, which also implies that the crack in the concrete is effectively controlled by the sprayable UHTCC. Owing to the recalibration of the ACI load factors in 2002 [42], the calculated maximum crack width of 0.4 mm (implicitly assumed by ACI before 1999) for the concrete structures was changed to 0.45 mm [43]. Thus, a crack width of 0.45 mm is employed as a reference in Fig. 12. It can be found that the maximum crack widths of UH10 and UH20 are below 0.45 mm, whereas that of UH0 is not. This also indicates that the sprayable UHTCC can be used to construct durable RC structures.

3.3. Test results of UH0, UH0 + 5, and UH0 + 10

As mentioned in Section 3.1, two more RC beams were pre-loaded using the average yield load of UH0 (approximately 55 kN). Then, the UHTCC layers were sprayed, and thereby, strengthened specimens UH0 + 5 and UH0 + 10 were obtained. The load *vs.* mid-span deflection curves of UH0 + 5 and UH0 + 10 are presented in Fig. 13. For the sake of comparison, the average curve of UH0 is also given. It can be seen that the strengthened specimens (i.e., UH0 + 5 and UH0 + 10) show a higher yield load and ultimate load compared with UH0. Additionally, the stiffness of the strengthened beams is higher than that of the control group. This indicates that the sprayable UHTCC can be considered as an ideal repair material for RC elements. The higher stiffness of UH0 + 5 and UH0 + 10 in Fig. 13 might be related to their larger sections compared to UH0. It should be noted that only one specimen was fabricated and tested for UH0 + 5 and UH0 + 10 in this study. For the sake of a more reliable conclusion, more specimens need

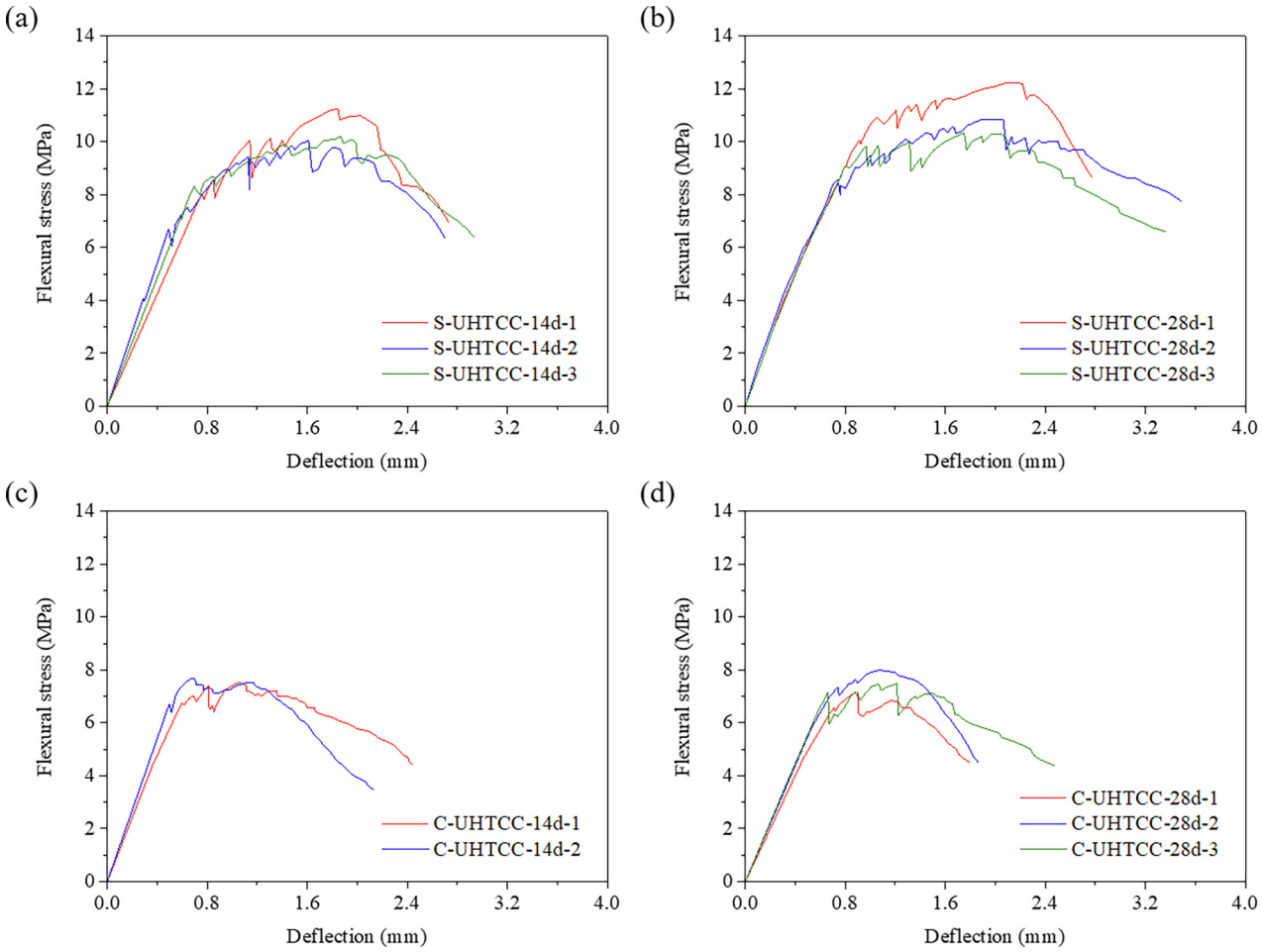

Fig. 7. Flexural stress *vs.* deflection curves: (a) sprayable UHTCC at 14 d; (b) sprayable UHTCC at 28 d; (c) cast UHTCC at 14 d; (d) cast UHTCC at 28 d.

to be tested in the following study to investigate this phenomenon. It needs to be pointed out that shear stresses will be induced along the interface of the concrete and sprayable UHTCCs owing to the tension in the UHTCC layer. In the experiment, only a slight debonding phenomenon is observed along the UHTCC/concrete interface because the tensile stress in the UHTCC is low. According to the above experimental results, for a 20-mm-UHTCC strengthened component, the interface treatment may be not necessary. However, the interface shear stress may become more remarkable as the thickness of the UHTCC layer increases. For that case, the UHTCC/concrete bonding strength may be not adequate. Some interface treatment methods should be applied to enhance the bonding strength. According to the former research of shotcrete jacketing concrete structures [44], some connecting techniques can be applied, which involves roughening the surface of the original concrete surface, embedding steel dowels into the original component and a combination of these two techniques. For the sprayed-UHTCC-strengthened system, these methods should be further experimentally investigated to check the effectiveness of the interface treatment in a following work.

3.4. Theoretical analysis

According to previous works [10,21], the flexural capacity of an RC beam strengthened by a UHTCC layer can be theoretically estimated. Two assumptions are used in the theoretical analysis: (1) strain along the section depth distributes linearly, and (2) the bond between the UHTCC and concrete as well as between a steel bar and concrete, is adequate. The following constitutive models of the UHTCC, concrete, and steel bar are used for the analysis.

For the UHTCC in tension, the bilinear constitutive model, which was proposed by Li et al. [3], is used. The model can be expressed as follows:

$$\sigma_t = \begin{cases} E_{UH}\varepsilon_t, & 0 \le \varepsilon_t \le \varepsilon_{t1} \\ \sigma_{t1}, & \varepsilon_{t1} \le \varepsilon_t \le \varepsilon_{t2} \end{cases} \quad (1)$$

where σ_t and ε_t are the tensile stress and strain, respectively; ε_{t1} is the cracking strain; ε_{t2} is the failure strain; E_{UH} is the tensile modulus; σ_{t1} is the tensile strength. For simplification, the stress after the cracking strain (ε_{t1}) is considered as a constant value (σ_{t1}). It needs to be pointed out that the tensile strain of the UHTCC at the steel-yield and ultimate stages of the beam specimen is higher than ε_{t1}; thus, only the values of σ_{t1} and ε_{t2} are used in the calculation of the load capacity (σ_{t1} = 1.9 MPa, ε_{t2} = 0.01).

For concrete in compression, the following model (Eq. (2)) is used for simplicity. A two-order parabola is used to describe the ascending segment, and constant value f_c is proposed for the descending branch.

$$\sigma_c = \begin{cases} f_c\left[2\frac{\varepsilon_c}{\varepsilon_0} - \left(\frac{\varepsilon_c}{\varepsilon_0}\right)^2\right], & 0 \le \varepsilon_c \le \varepsilon_0 \\ f_c, & \varepsilon_0 \le \varepsilon_c \le \varepsilon_{cu} \end{cases} \quad (2)$$

where σ_c and ε_c are the compressive stress and strain, respectively; ε_0 is 0.002; ε_{cu} is the failure strain (0.0033); f_c is the compressive strength of concrete (26.7 MPa).

For a steel bar, the perfect elastic-plastic model is used (Eq. (3)), and the strain-hardening response is not considered.

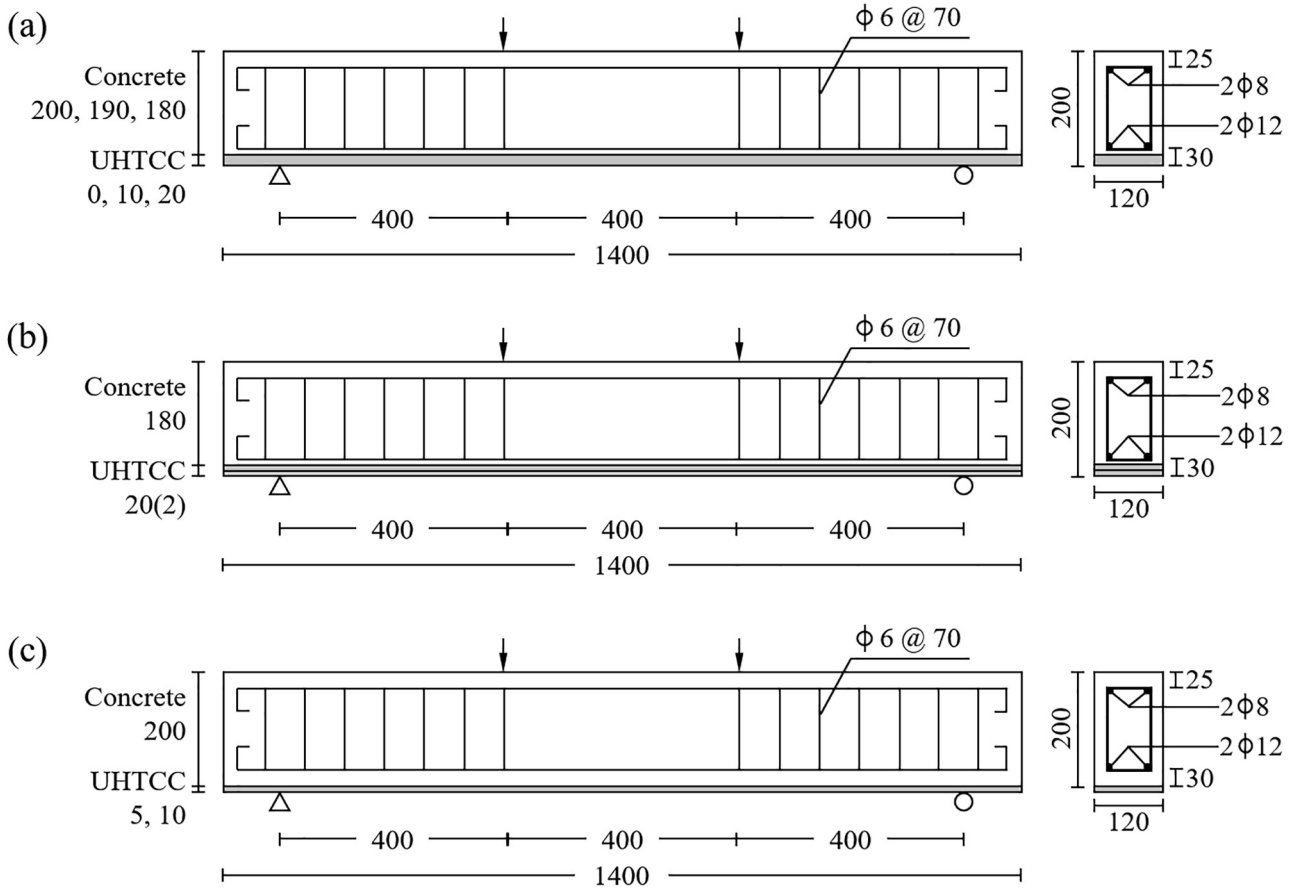

Fig. 8. Specimen details and test set-up of the four-point bending test: (a) sprayable-UHTCC-strengthened RC beams; (c) sprayable-UHTCC-strengthened pre-loaded RC beams.

$$\sigma_s = \begin{cases} E_s\varepsilon_s, & 0 \le \varepsilon_s \le \varepsilon_y \\ f_y, & \varepsilon_y \le \varepsilon_s \le \varepsilon_{s,h} \end{cases} \tag{3}$$

where σ_s and ε_s are the steel stress and strain, respectively; ε_y is the yield strain; $\varepsilon_{s,h}$ is the failure strain; E_s is the tensile modulus; f_y is the yield strength. During the calculation of the steel-yield and ultimate capacities of the beam specimen, $\varepsilon_y = 0.002$ and $f_y = 391$ MPa are used for the bars in tension, and $E_s = 200$ GPa is used for the bars in compression (not yield until specimen failure).

On the basis of the above assumption and constitutive models of the materials, the distributions of strain and stress along the specimen section can be obtained at the steel-yield and ultimate stages, which are shown in Fig. 14. At the steel-yield stage, the strain of the steel bars in tension is ε_y and strain of concrete at the top of the section is lower than ε_0 (see Fig. 14(a)). At the ultimate stage, the strain of the UHTCC is ε_{t2} and strain of concrete at the top is between ε_0 and ε_{cu} (shown in Fig. 14(b)). According to the distributions of the strain and stress, the equilibrium equations of the force (N) and moment (M) at each stage can be obtained as follows:

$$\begin{cases} \sum N = 0 \Rightarrow ab\sigma_t + \sigma_{st}A_{st} - \int_c^h b\sigma_c dx - \sigma_{sc}A_{sc} = 0 \\ \sum M = 0 \Rightarrow \frac{1}{2}a^2b\sigma_t + \sigma_{st}A_{st}m - \int_c^h b\sigma_c x dx - \sigma_{sc}A_{sc}n + M = 0 \end{cases} \tag{4}$$

where a is the thickness of UHTCC layer; b and h are the width and height of the beam section; c is the location of the neutral axis; m and n are the locations of the steel bars in tension and compression, respectively; σ_{st} and σ_{sc} are the stresses of the steel bars in tension and compression, respectively; A_{st} and A_{sc} are the section areas of the steel bars in tension and compression, respectively.

The load capacity of an RC beam-strengthened by the UHTCC layer can be calculated based on Eq. (4). The tested and calculated loads at the steel-yield and ultimate stages of each group specimens are listed in Table 4. It can be observed that the deviation between the calculated and tested loads of each group ranges from −9.0% to 11.1%. The prediction errors seem not large, but there are still several limitations of this theoretical analysis. The calculation results of the loads are proportional to the thickness of UHTCC layer, but the tested yield-load increase from UH10 to UH20 is much larger than that from UH0 to UH10. There might be some fabrication errors of the beam specimens

Table 3
Specimen ID and dimensions.

Description	Specimen ID	UHTCC layer (mm)	Number	Final dimensions (mm)
RC beams with UHTCC	UH0	0	2	120 × 200 × 1400
	UH10	10 (one layer)	2	
	UH20	20 (one layer)	2	
	UH20(2)	20 (two layers)	1	
Pre-loaded RC beams with UHTCC	UH0 + 5	5 (one layer)	1	120 × 205 × 1400
	UH0 + 10	10 (one layer)	1	120 × 210 × 1400

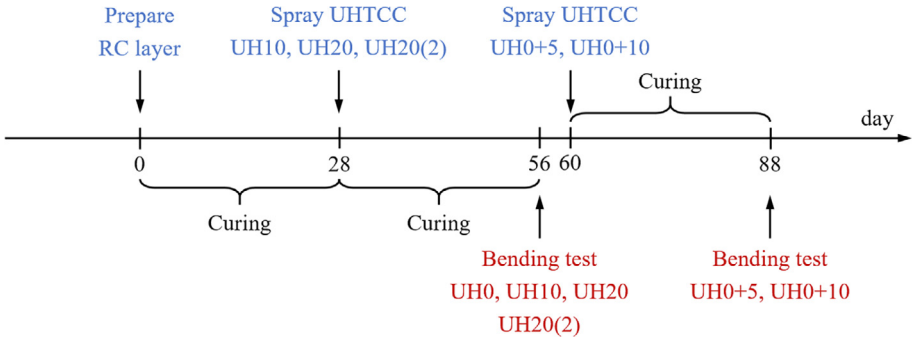

Fig. 9. Timeline of the specimen preparation and bending test.

and the mechanical parameters obtained by the material tests might have some variations. These reasons may affect the prediction of the yield load. Additionally, it can be seen that the ultimate loads of all the specimens are a little underestimated (on the safe side). This phenomenon may be related to the simplified tensile constitutive models of UHTCC and steel bars, because the strain-hardening responses are not considered. In the following study, further work is needed to investigate the reliability and accuracy of this method.

For practical applications, sprayable UHTCCs with various strengths and thicknesses may be utilized. Hence, on the basis of the above method, the load capacity of an RC beam strengthened by other different UHTCC layers under the same loading condition can also be obtained. Fig. 15 presents the calculated steel-yield loads of these RC-UHTCC beams. It needs to be pointed out that the RC layer of the beam section in Fig. 15 is similar to that of the pre-loaded RC beam in Fig. 8(c). The thickness of the UHTCC layer ranges from 0 to 30 mm. The tensile strength of the UHTCC ranges from 1.9 MPa to 5 MPa. It can be found that the steel-yield load of the section increases practically linearly as the tensile strength and thickness of the UHTCC increase. If an RC beam is strengthened by a 30-mm-UHTCC layer with a tensile strength of 5 MPa, the flexural load capacity can be improved by 27% compared to the original RC beam. It should be noted that tension in the UHTCC increases as the thickness and strength of the UHTCC increase during the bending test, which may result in a remarkable debonding along the UHTCC/concrete interface. Hence, in those cases, some interface treatment methods should be applied to enhance the

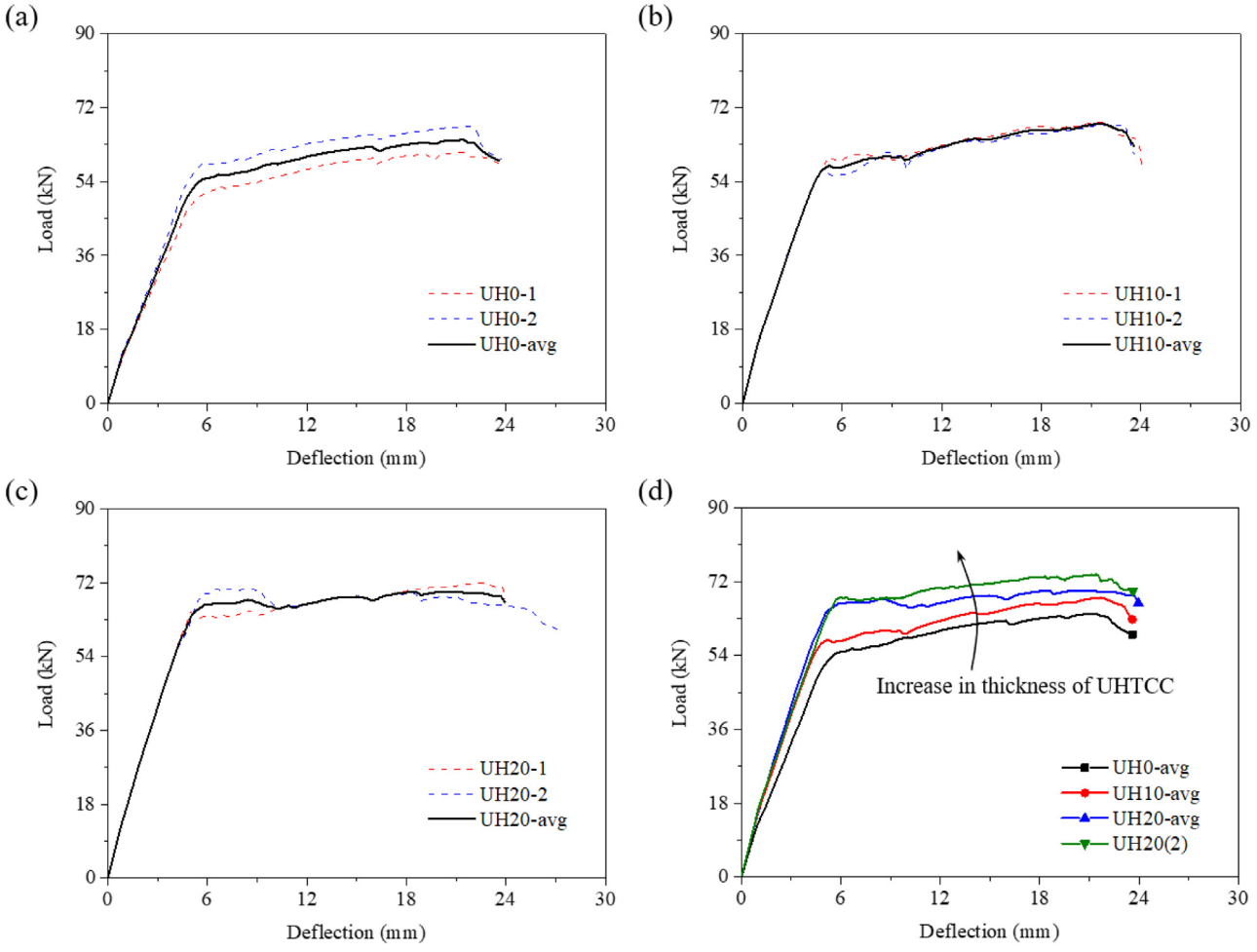

Fig. 10. Load–deflection curves of the sprayable-UHTCC-strengthened RC beams: (a) UH0; (b) UH10; (c) UH20; (d) comparison of the average curves and UH20(2).

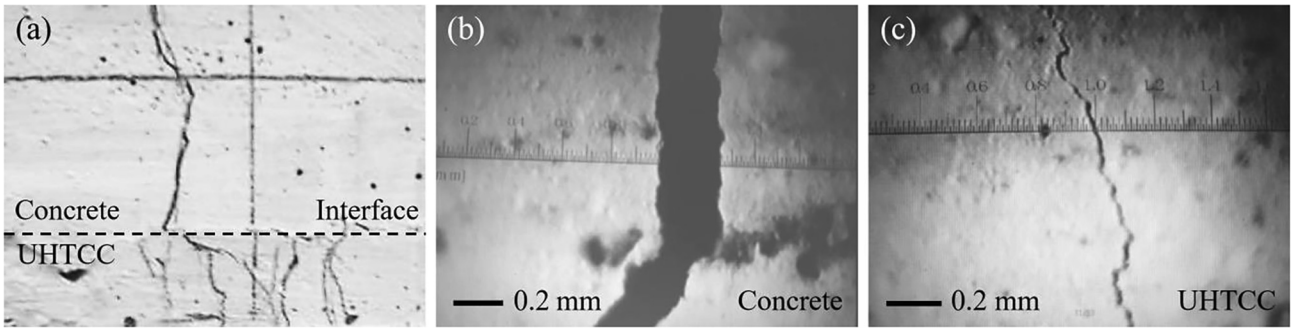

Fig. 11. Local cracks in specimen UH20 at the load of 60 kN: (a) cracking mode; (b) crack at the concrete layer; (c) crack at the UHTCC layer.

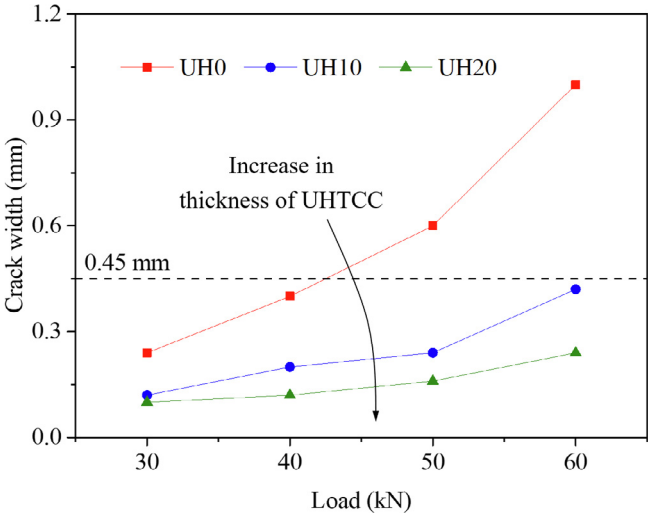

Fig. 12. Crack widths in the concrete layers of the sprayable-UHTCC-strengthened RC beams.

bonding performance of the UHTCC/concrete interface.

On the basis of the experimental and theoretical results in this section, it can be concluded that this sprayed-UHTCC-strengthened system can be mainly applied to improve the durability of concrete structures owing to the good crack-control ability of UHTCC, while the loading capacity of the strengthened component is only partially improved.

4. Application cases of sprayable UHTCCs in China

A sprayable UHTCC can be applied in the construction of high-durability concrete structures and restoration of aged concrete structures as a surface protection layer owing to the high ductility and fine cracking mode of this material. In this section, two application cases using the sprayable UHTCC will be briefly introduced.

In the first case, the sprayable UHTCC was used to strengthen the second lining of the Xinling tunnel (Zhejiang, China), which is shown in Fig. 16. The average length of the Xinling tunnel is 1423 m. For one tunnel, the width is 10.75 m and height is 5.0 m. The UHTCC material is sprayed to form a protective layer after the construction of the second lining of the tunnel. The sprayable UHTCC layer is expected to control the crack of the concrete layer and delay the deterioration of the structure. In this case, a 20-mm-UHTCC layer is sprayed, and the

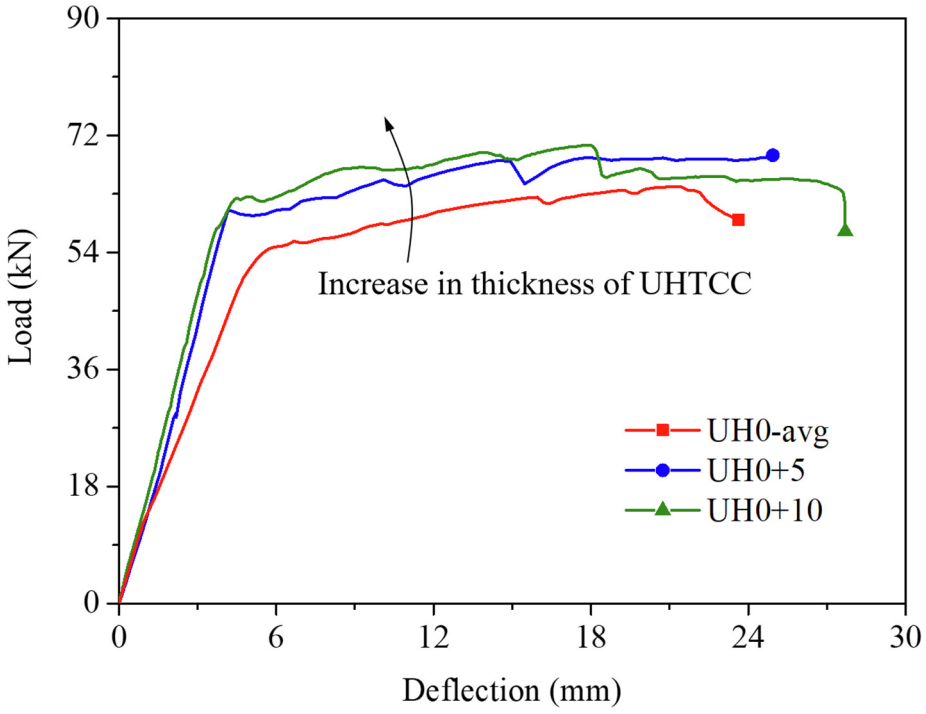

Fig. 13. Load–deflection curves of the sprayable-UHTCC-strengthened pre-loaded RC beams.

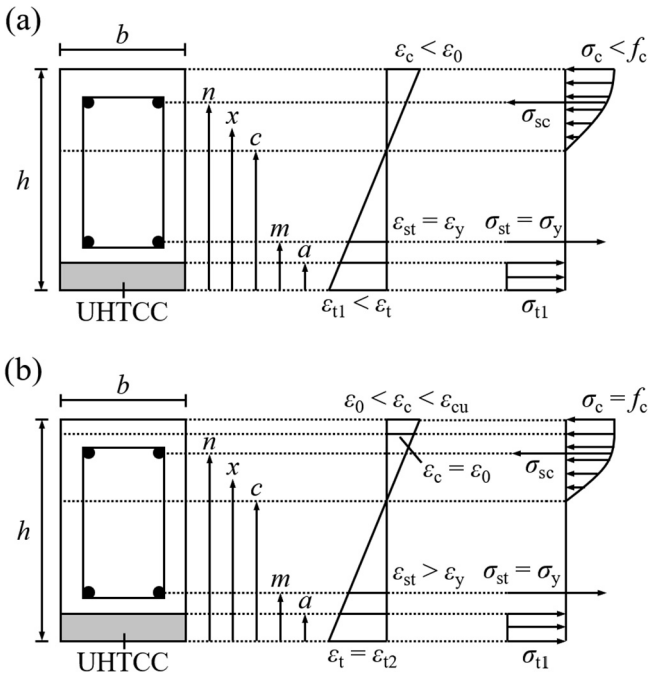

Fig. 14. Distributions of the strain and stress along the specimen section at (a) steel-yield stage and (b) ultimate stage.

construction process can be seen in Fig. 16. First, the surface of the constructed second lining is cleaned using water jetting of 2 MPa. Second, the UHTCC is sprayed using the air flow of approximately 0.09 m^3/min to 0.2 m^3/min and the air pressures of 650 kPa to 300 kPa. Finally, the surface of the sprayable UHTCC is smoothed. Fig. 16(d) presents the Xinling tunnel open to traffic.

In the second case, the sprayable UHTCC was applied in the restoration of the bottom slab of the Changshangang bridge (Zhejiang, China). Flexural fatigue cracks are found at the bottom slab of this bridge, and thus, the sprayable UHTCC is applied to control the cracks and improve the durability of the structures. A 20-mm-UHTCC layer with an area of 800 m^2 is sprayed, and the restoration in this case is finished under open traffic. A similar spray process is also applied during the restoration (shown in Fig. 17).

5. Conclusions

In this paper, a systematical investigation of sprayable UHTCC strengthening a reinforced concrete structure was presented. It was found that a narrow stream of the sprayable UHTCC could be achieved with an air flow of approximately 0.3 m^3/min and an air pressure of 200 kPa, whereas a foggy-like sprayable UHTCC could be obtained with an air flow of approximately 0.1 m^3/min and an air pressure of 600 kPa. The compressive, tensile, and flexural strengths of the sprayable UHTCC were higher than those of the cast UHTCC having the same proportion. In the four-point bending tests of the RC–UHTCC beams, it was found

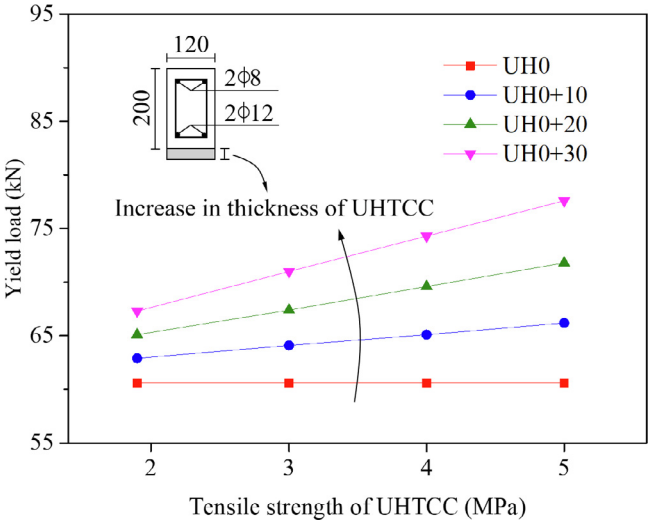

Fig. 15. Calculated steel-yield loads of the RC beams strengthened by the UHTCCs of various strengths and thicknesses.

Fig. 16. Strengthening of the second lining of the Xinling tunnel (Zhejiang, China) using the sprayable UHTCC: (a) UHTCC is sprayed; (b) surface is smoothened; (c) construction is completed; (d) tunnel is open to traffic.

that the stiffness, steel yield load, and ultimate load of the beam specimens increased as the thickness of the UHTCC layer increased, and the sprayable UHTCC layer could effectively control the crack occurring

Table 4
Tested and calculated loads at the steel-yield and ultimate stages.

Specimen ID	Steel-yield load (kN)		Variation (%)	Ultimate load (kN)		Variation (%)
	Calculation	Test-avg		Calculation	Test-avg	
UH0	60.9	54.8	11.1	63.3	64.1	−1.2
UH10	62.8	57.8	8.7	65.2	68.5	−4.8
UH20	64.6	66.5	−2.9	67.1	70.2	−4.4
UH20(2)	64.6	67.8	−4.7	67.1	73.7	−9.0
UH0 + 5	61.9	60.6	2.1	64.3	68.1	−5.6
UH0 + 10	62.9	62.3	1.0	65.3	70.4	−7.2

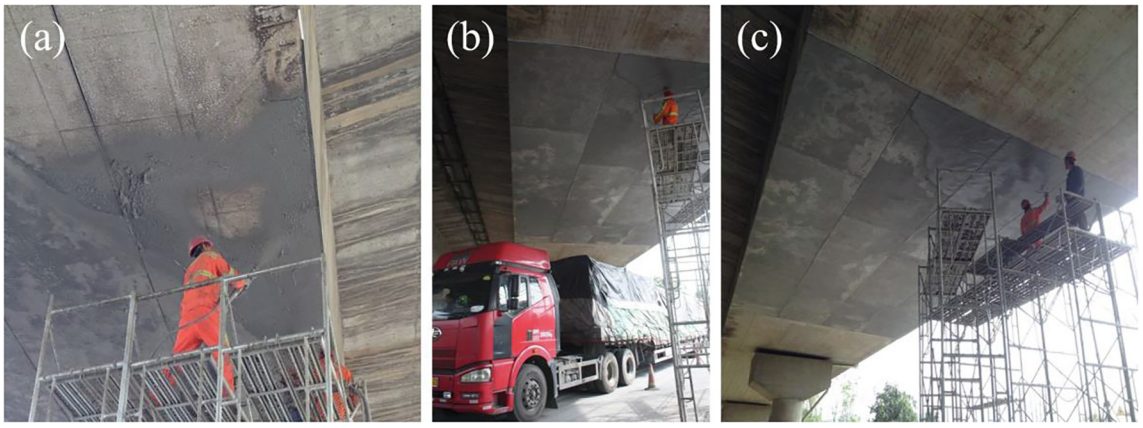

Fig. 17. Restoration of the bottom slab of the Changshangang bridge (Zhejiang, China) using the sprayable UHTCC: (a) UHTCC is sprayed; (b) restoration is done under open traffic; (c) surface is smoothened.

in concrete layer. In addition, the layer-by-layer spray process for the UHTCC did not affect the load capacity of the beam specimen as opposed to the single-layer spray process. The results of the theoretical analysis showed a good coincidence with those of the bending tests, and this method could be used to predict the load capacity of the RC–UHTCC beams. In summary, this strengthening system based on the sprayable UHTCC can be mainly applied to improve the durability of concrete structures owing to the crack-control ability of UHTCC, while the loading capacity of the strengthened component can only be partially improved. Finally, the application cases (i.e., tunnel and bridge) of the sprayable UHTCC in China exhibited the potential applications of this material in the construction of durable concrete structures and restoration of aged structures.

Acknowledgments

The authors would like to acknowledge the financial support provided by the National Natural Science Foundation of China under Grant Nos. 51622811 and 51678522. The authors also thank Mr. Xiao-Hua Ji and Mr. Yu Peng at the College of Civil Engineering and Architecture of Zhejiang University for their support in the experiments. The authors appreciate the efforts of the anonymous reviewers to improve the quality of this study.

References

[1] Li VC, Leung CK. Steady-state and multiple cracking of short random fiber composites. J Eng Mech-ASCE 1992;118(11):2246–64.
[2] Li VC. From micromechanics to structural engineering-the design of cementitious composites for civil engineering applications. J Struct Mech Earthquake Eng 1993;10(2):37–48.
[3] Li VC, Wang S, Wu C. Tensile strain-hardening behavior of polyvinyl alcohol engineered cementitious composite (PVA-ECC). ACI Mater J 2001;98(6):483–92.
[4] Yu J, Li H, Leung CK, Lin X, Lam JY, Sham IM, et al. Matrix design for waterproof engineered cementitious composites (ECCs). Constr Build Mater 2017;139:438–46.
[5] Yu KQ, Yu JT, Dai JG, Lu ZD, Shah SP. Development of ultra-high performance engineered cementitious composites using polyethylene (PE) fibers. Constr Build Mater 2018;158:217–27.
[6] Li VC, Hashida T. Engineering ductile fracture in brittle-matrix composites. J Mater Sci Lett 1993;12(12):898–901.
[7] Yu J, Yao J, Lin X, Li H, Lam JY, Leung CK, et al. Tensile performance of sustainable Strain-Hardening Cementitious Composites with hybrid PVA and recycled PET fibers. Cem Concr Res 2018;107:110–23.
[8] Lin X, Yu J, Li H, Lam JY, Shih K, Sham IM, et al. Recycling polyethylene terephthalate wastes as short fibers in strain-hardening cementitious composites (SHCC). J Hazard Mater 2018;357:40–52.
[9] Li H, Xu S, Leung CKY. Tensile and flexural properties of ultra high toughness cemontious composite. J Wuhan Univ Technol-Mater Sci Ed 2009;24(4):677–83.
[10] Li QH, Huang BT, Xu SL. Development of assembled permanent formwork using ultra high toughness cementitious composites. Adv Struct Eng 2016;19(7):1142–52.
[11] Huang BT, Li QH, Xu SL, Zhou BM. Frequency effect on the compressive fatigue behavior of ultrahigh toughness cementitious composites: experimental study and probabilistic analysis. J Struct Eng-ASCE 2017;143(8):04017073.
[12] Suthiwarapirak P, Matsumoto T, Kanda T. Multiple cracking and fiber bridging characteristics of engineered cementitious composites under fatigue flexure. J Mater Civ Eng-ASCE 2004;16(5):433–43.
[13] Zhou J, Pan J, Leung CK. Mechanical behavior of fiber-reinforced engineered cementitious composites in uniaxial compression. J Mater Civ Eng-ASCE 2014;27(1):04014111.
[14] Li QH, Huang BT, Xu SL, Zhou BM, Yu RC. Compressive fatigue damage and failure mechanism of fiber reinforced cementitious material with high ductility. Cem Concr Res 2016;90:174–83.
[15] Huang BT, Li QH, Xu SL, Zhou BM. Tensile fatigue behavior of fiber-reinforced cementitious material with high ductility: experimental study and novel P-S-N model. Constr Build Mater 2018;178:349–59.
[16] Huang BT, Li QH, Xu SL. Fatigue deformation model of plain and fiber-reinforced concrete based on the Weibull function. J Struct Eng-ASCE 2019;145(1):04018234.
[17] Huang BT, Li QH, Xu SL, Liu W, Wang HT. Fatigue deformation behavior and fiber failure mechanism of ultra-high toughness cementitious composites in compression. Mater Des 2018;157:457–68.
[18] Li VC, Kanda T. Innovations forum: engineered cementitious composites for structural applications. J Mater Civ Eng-ASCE 1998;10(2):66–9.
[19] Li VC, Horii H, Kabele P, Kanda T, Lim YM. Repair and retrofit with engineered cementitious composites. Eng Fract Mech 2000;65(2–3):317–34.
[20] Leung CKY, Cao Q. Development of pseudo-ductile permanent formwork for durable concrete structures. Mater Struct 2010;43(7):993–1007.
[21] Huang BT, Li QH, Xu SL, Li CF. Development of reinforced ultra-high toughness cementitious composite permanent formwork: experimental study and Digital Image Correlation analysis. Compos Struct 2017;180:892–903.
[22] Huang BT. Fatigue performance of strain-hardening fiber-reinforced cementitious composite and its functionally-graded structures Ph.D. thesis Zhejiang University; 2018.
[23] Maalej M, Li VC. Introduction of strain-hardening engineered cementitious composites in design of reinforced concrete flexural members for improved durability. ACI Struct J 1995;92(2):167–76.
[24] Maalej M, Ahmed SF, Paramasivam P. Corrosion durability and structural response of functionally-graded concrete beams. J Adv Concr Technol 2003;1(3):307–16.
[25] Kim YY, Kong HJ, Li VC. Design of engineered cementitious composite suitable for wet-mixture shotcreting. ACI Mater J 2003;100(6):511–8.
[26] Kanda T, Saito T, Sakata N, Hiraishi M. Tensile and anti-spalling properties of direct sprayed ECC. J Adv Concr Technol 2003;1(3):269–82.
[27] Kim YY, Fischer G, Lim YM, Li VC. Mechanical performance of sprayed engineered cementitious composite using wet-mix shotcreting process for repair applications. ACI Mater J 2004;101(1):42–9.
[28] Kim YY. Repair performance of engineered cementitious composites (ECC) treated with wet-mix spraying process. Int J Concr Struct Mater 2006;18(3E):207–11.
[29] Rokugo K, Kanda T, Yokota H, Sakata N. Applications and recommendations of high performance fiber reinforced cement composites with multiple fine cracking (HPFRCC) in Japan. Mater Struct 2009;42(9):1197.
[30] Li VC, Fischer G, Lepech M. Shotcreting with ECC. In: Kusterle W, editor. Proceedings CD. Austria: Spritzbeton-Tagung; 2009.
[31] Zhang Q, Li VC. Development of durable spray-applied fire-resistive engineered cementitious composites (SFR-ECC). Cem Concr Compos 2015;60:10–6.
[32] ACI Committee 506. Guide to Shotcrete (ACI 506R-16), American Concrete Institute; 2016.
[33] EFNARC. European Specification for Sprayed Concrete. EFNARC, 1996.
[34] Japan Society of Civil Engineers. Recommendations for design and construction of high performance fiber reinforced cement composites with multiple fine cracks (HPFRCC). Concrete Engineering Series 82, 2008.
[35] Lukkarila MR. Low-Velocity Spraying of Cementitious Materials – Is It Shotcrete? Summer: Shotcrete Magazine - American Shotcrete Association; 2006. p. 50–1.
[36] ASTM C. Standard test method for density, absorption, and voids in hardened concrete. C642-13, 2013.
[37] Austin SA, Robins PJ, Goodier CI. The performance of hardened wet-process

sprayed mortars. Mag Concr Res 2000;52(3):195–208.
[38] Maalej M, Li VC. Flexural/tensile-strength ratio in engineered cementitious composites. J Mater Civ Eng 1994;6(4):513–28.
[39] Chen Z, Yang EH, Yang Y, Yao Y. Latex-modified engineered cementitious composites (L-ECC). J Adv Concr Technol 2014;12(12):510–9.
[40] Wang S, Li VC. Tailoring of pre-existing flaws in ECC matrix for saturated strain hardening Vail, Colorado, USA Proceedings of 5th International Conference on Fracture Mechanics of Concrete and Concrete Structures (FraMCoS-5)2004. p. 1005–12.
[41] Kim YY, Lee BY, Bang JW, Han BC, Feo L, Cho CG. Flexural performance of reinforced concrete beams strengthened with strain-hardening cementitious composite and high strength reinforcing steel bar. Compos B Eng 2014;56:512–9.
[42] American Concrete Institute (ACI) Committee 318. Building code requirements for structural concrete and commentary ACI 318-08/ACI 318R-08, Farmington Hills, MI; 2008.
[43] Harries KA, Shahrooz BM, Soltani A. Flexural crack widths in concrete girders with high-strength reinforcement. J Bridge Eng-ASCE 2011;17(5):804–12.
[44] Vandoros KG, Dritsos SE. Interface treatment in shotcrete jacketing of reinforced concrete columns to improve seismic performance. Struct Eng Mech 2006;23(1):43–61.